Chapter 30
Density Functional Study of the Origin of the Strongly Delocalized Electronic Structure of the Cu_A Site in Cytochrome *c* Oxidase

Yu Takano, Orio Okuyama, Yasuteru Shigeta, and Haruki Nakamura

Abstract The Cu_A site is the electron entrance of cytochrome *c* oxidase (C*c*O), the terminal redox-driven proton pump in mitochondria and aerobic bacteria. The ground state of the oxidized Cu_A site is related to the singly occupied molecular orbital, since the Cu_A site is doublet in the oxidized state. Spectroscopic studies have suggested the strongly delocalized character of the σ_u* oxidized ground state of the Cu_A site facilitates a rapid electron transfer to heme *a* in C*c*O. We address the origin of the strongly delocalized character of the Cu_A site, using the density functional theory. Our computation shows that the fully delocalized mixed-valence $Cu^{1.5+}$–$Cu^{1.5+}$ species is due to the direct interaction between the two copper ions of the Cu_A site and the stabilization of the Cu–Cu interaction by the ligand coordination. In addition, the Cu_A site holds the equivalent shapes of the σ_u* redox active molecular orbital and spin density distribution, despite the structural deformation of the Cu_2S_2 core. It indicates that the Cu_A site has a character of "flexible electron mediator," as well as heme *a*. This character is common to transition metal cofactors involving in electron transfer in biology.

30.1 Introduction

The Cu_A site functions as an electron transfer intermediate in cytochrome *c* oxidase (C*c*O), the terminal electron acceptor in aerobic respiration [1–6]. The geometrical and electronic properties of the Cu_A site in C*c*O have been studied by

Y. Takano (✉) • O. Okuyama • H. Nakamura
Institute for Protein Research, Osaka University, Suita, Osaka 565-0871, Japan
e-mail: ytakano@protein.osaka-u.ac.jp; okuyama@protein.osaka-u.ac.jp; harukin@protein.osaka-u.ac.jp

Y. Shigeta
Graduate School of Engineering Science, Osaka University, Suita, Osaka 565-0871, Japan
e-mail: shigeta@cheng.es.osaka-u.ac.jp

K. Nishikawa et al. (eds.), *Quantum Systems in Chemistry and Physics*,
Progress in Theoretical Chemistry and Physics 26, DOI 10.1007/978-94-007-5297-9_30,

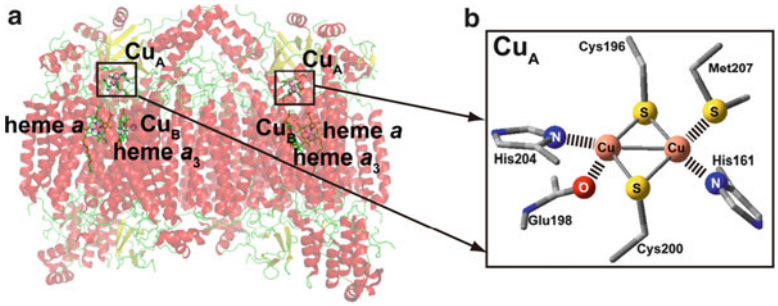

Fig. 30.1 The X-ray crystallographic structure of cytochrome *c* oxidase (C*c*O) (**a**) and the Cu_A site (**b**) (PDB ID: 1V54)

X-ray crystallography, electron paramagnetic resonance (EPR), X-ray absorption (XAS), resonance Raman (rR), extended X-ray absorption fine structure (EXAFS), magnetic circular dichroism (MCD), and nuclear magnetic resonance (NMR) spectroscopies, as well as by density functional theory (DFT), suggesting that the Cu_A site adopts a characteristic molecular structure [7–21].

The X-ray crystallographic structures of C*c*O revealed that the Cu_A site contains two copper ions bridged by two cysteinyl thiolate groups, and that each copper ion is coordinated equatorially with a histidine residue and axially with either a methionine residue or a carbonyl group of the polypeptide backbone (Fig. 30.1b) [7]. The Cu–Cu distance is remarkably short enough to allow the formation of a direct bond between the two copper ions. An EXAFS and parallel MCD studies supported the occurrence of direct Cu–Cu bonding in the Cu_A site [8, 9]. The reduced Cu_A site has a Cu^{1+}–Cu^{1+} core, which is oxidized by one electron. EPR studies demonstrated that the Cu_A site is a completely delocalized mixed-valence $Cu^{1.5+}$–$Cu^{1.5+}$ species [10–14]. Many synthetic modeling studies also elucidated the important structural features for electronic and functional properties of the Cu_A site [15–17]. Tolman and collaborators synthesized a model complex [15, 16]. The complex shows a mixed-valence oxidized state, as well as the Cu_A site, but has a longer Cu–Cu distance of 2.9 Å, which implies no direct Cu–Cu bond interaction [15]. XAS and absorption spectra of the synthetic model suggested stronger superexchange interactions via the bridging thiolate groups but a weaker Cu–Cu electronic coupling [16]. On the other hand, a combination of rR and XAS of the Cu_A site showed that both the direct Cu–Cu interaction and the superexchange interactions via the Cu–S bonds contribute to the electronic coupling between the two copper ions [10]. DFT calculations also revealed that the mixed-valence synthetic model has a singly occupied π_u redox active molecular orbital (RAMO), while that the oxidized Cu_A site shows a completely delocalized σ_u* ground state, in which an unpaired electron occupies the σ_u* RAMO, as illustrated in Fig. 30.2 [10, 16, 18–21]. The completely delocalized σ_u* RAMO produces the stronger electronic coupling between two copper ions, which provides a strongly stabilized and delocalized electronic structure. This electronic structure greatly contributes to

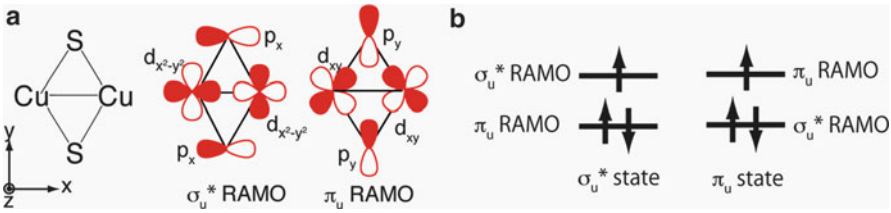

Fig. 30.2 Schematic pictures of the σ_u* and π_u redox active molecular orbitals (RAMOs) (**a**) and the σ_u* and π_u states (**b**)

maintain the Cu_A site delocalized in the low-symmetry protein environment. Olsson and Ryde also conducted DFT calculations on the Cu_A site, concluding that the delocalization of the unpaired electron causes the lowering of the reorganization energy in the mixed-valence oxidized state [19]. The complete delocalization of an unpaired electron and the small reorganization energy result in the rapid electron transfer rates.

Our ultimate goal is to elucidate the origin of the characteristic electronic structure of the transition metal centers in proteins and its regulation by a protein environment. As shown in our recent studies [22–29], we have found that the protein environment enhances the intrinsic abilities of the cofactor. Thus, our computation suggests that a study of the intrinsic electronic structure of the cofactor is essential to understand the function of metalloproteins. For example, the redox reaction of heme *a* itself causes the charge transfer from the Fe ion to the heme propionate, and the surrounding protein environment enlarges the charge transfer in C*c*O [22, 23]. We also reported the protein activation of the electronic asymmetry of a special pair cation radical in the photosynthetic reaction center [24] and the increased reactivities of hemerythrin and hemocyanin, by the surrounding protein residues [25–27].

In the previous studies [20, 21], the electronic structures of various models of the Cu_A site have been examined by using the DFT methods to elucidate what are required and sufficient to form the characteristic σ_u* ground state of the Cu_A site. We first explored the electronic structure of the Cu_2S_2 core model, which consists of two copper ions and two deprotonated Cys residues [20]. Our computation of the oxidized Cu_2S_2 core model revealed that the π_u state is more stable than the σ_u* state, even in the short Cu–Cu distance. An addition of the coordinating ligands to Cu_2S_2 core model leads to the σ_u* ground state, due to electrostatic and orbital interactions between the core and the ligands, and implies that not only the direct Cu–Cu interaction but also the electrostatic and the orbital interactions by ligand coordination are responsible for the stabilization of the σ_u* state rather than the π_u state in the Cu_A site. We next examined the effects of each coordinating ligand on the electronic structures of the Cu_A site through DFT calculations [21]. His ligation provides both strong orbital and electrostatic interactions to the Cu_2S_2 core, dominating both stabilization of the σ_u* ground state and regulation of the ionization potential of the Cu_A site. The coordination of the peptide carbonyl

group electrostatically affects the ionization potential. Weak orbital and electrostatic interactions by the Met coordination are influential to the stabilization of the σ_u* ground state.

In the present study, we address the origin of the strong delocalized character of the oxidized σ_u* ground state in the Cu_A site, using the DFT method (the M06 exchange–correlation functional). In particular, we have examined the RAMOs, spin density distribution, and Mulliken atomic spin and charge densities of the models of the Cu_A site in the σ_u* and π_u states. Our computation demonstrates that the direct Cu–Cu bond and the ligand coordination lead to the strong and robust delocalization over the Cu_2S_2 core in the Cu_A site even with the structural deformation of the Cu_2S_2 core. It indicates that the Cu_A site has a character of "flexible electron mediator." This character is also found in heme *a* [23], implying that the robustness to the structural distortion is required to transition metal cofactors involved in biological electron transfer.

30.2 Computational Procedure

30.2.1 Model Construction

The models for the oxidized Cu_A site were constructed with the three-dimensional atomic structure of fully oxidized bovine heart C*c*O at the 1.8 Å resolution (PDB ID: 1V54), while the reduced Cu_A site was modeled with fully reduced bovine heart C*c*O at the 1.9 Å resolution (PDB ID: 1V55). Bovine heart C*c*O is dimerized, and each monomer consists of 13 subunits. Subunit II, which is represented by chain B and O in PDB data of bovine heart C*c*O, contains the Cu_A site. Since the Cu–Cu distances of chain B and O are quite different from each other, the 1V54B, 1V54O, 1V55B, and 1V55O models were built for the Cu_A site in the chain B and O of the oxidized and reduced C*c*O, respectively, as illustrated in Fig. 30.3a. The geometrical parameters of two copper ions, the bridging Cys residues, Cys196 and Cys200, and the coordinating amino acids, His161, Glu198, His204, and Met207, were employed for the construction of the models. In the models, each C_α atom of His161, Cys196, Cys200, His204, and Met207 was replaced with an H atom, and Glu198 was replaced with *N*-methyl acetamide. We classified the models into the core, His161, Glu198, His204, and Met207 parts, according to the Cu_2S_2 core and the coordinating ligands, as illustrated in Fig. 30.3b. The positions of the hydrogen atoms were optimized, while the heavy atoms were fixed to the positions in the corresponding X-ray structure.

30.2.2 Quantum Chemical Calculations

All quantum chemical calculations were performed on the models with the Gaussian 09 program packages [30]. In the previous study [20], we assessed the validity of

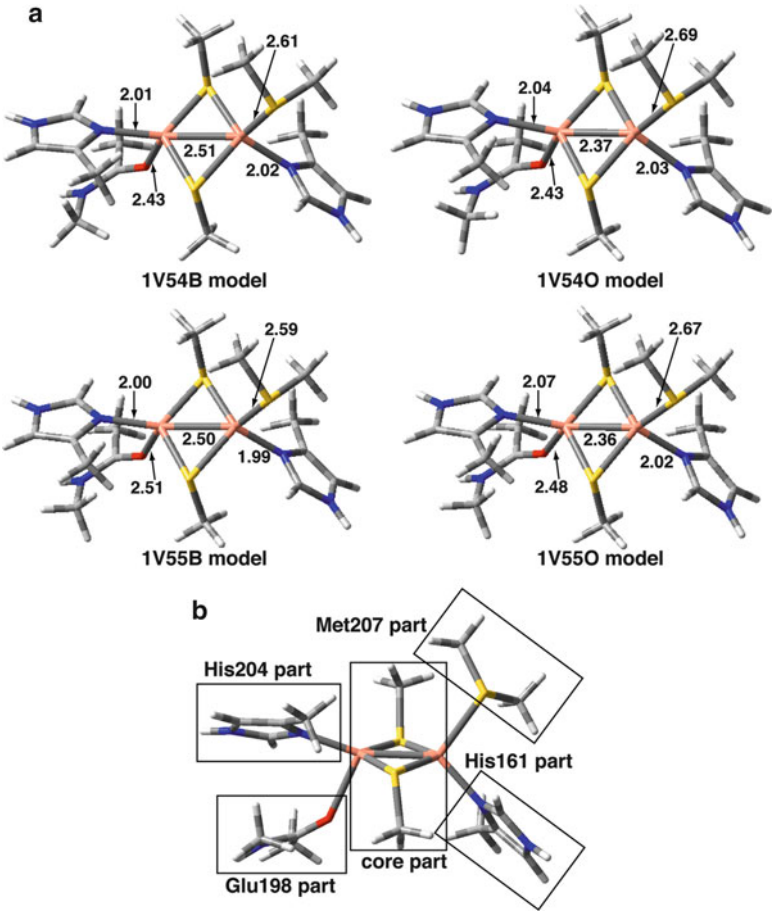

Fig. 30.3 Models of the Cu_A site, the 1V54B, 1V54O, 1V55B, and 1V55O models (**a**), and the classification of the models into the core, His161, Glu198, His204, and Met207 parts, according to the Cu_2S_2 core and the coordinating ligands (**b**)

exchange–correlation functionals of DFT (BHandHLYP [31], B3LYP [32], BLYP [33, 34], PW91 [35], PBE0 [36], and M06 [37]) in comparison to the coupled cluster (CC) methods [38] and demonstrated that the M06 exchange–correlation functional [39] can be regarded as a reliable method to examine the electronic structure of the Cu_2S_2 core. The M06 exchange–correlation functional was employed for the investigation of the electronic structures of the Cu_A site. We used the Wachters + f basis sets for copper ions [40] and the Pople's 6-311++G(df,pd) basis sets for other atoms [41, 42]. The environmental effect inside the protein was computed with PCM using UAKS cavity [43, 44] with a dielectric constant of 4.0 [45, 46]. The accuracy of PCM heavily depends on the use of proper boundary conditions on

the surface of the cavity containing solutes. In the present study, the UAKS cavities were used in the PCM calculations since it provides reliable solvation energies for many molecules and ions [44].

30.3 Results and Discussion

30.3.1 Redox Active Molecular Orbitals (RAMOs) of the Cu_A Site

We first examined the shapes and symmetries of the RAMOs of the oxidized models (the 1V54B and 1V54O models) in the σ_u* and π_u oxidized states. The RAMOs are represented by β-LUMOs and are equivalent to the singly occupied molecular orbitals (SOMOs). Figure 30.4 illustrates the RAMOs of the 1V54B and 1V54O models in the σ_u* and π_u oxidized states. The σ_u* RAMOs consist of an antibonding orbital between a dσ* orbital (d_{x2-y2}–d_{x2-y2}) of the Cu–Cu part and a pπ orbital ($p_x + p_x$) of the S–S part of the Cu_2S_2 core in the Cu_A site, as illustrated in Fig. 30.2a. On the other hand, the π_u RAMOs are composed of an antibonding orbital interaction between a dπ orbital ($d_{xy} + d_{xy}$) of the Cu–Cu part and a pσ* orbital (p_y–p_y) of the S–S part of the Cu_2S_2 core in the Cu_A site (Fig. 30.2a).

As shown in Fig. 30.4, the σ_u* RAMOs are delocalized on the coordinating ligands, the N_δ atoms of His161 and His204 and the S_γ atom of Met207, and exhibit antibonding orbital interactions between the Cu_2S_2 core and the coordinating ligands. These antibonding orbital interactions indicate the increase in the σ_u* RAMO energy. In contrast to the σ_u* RAMOs, the π_u RAMOs of all of the models

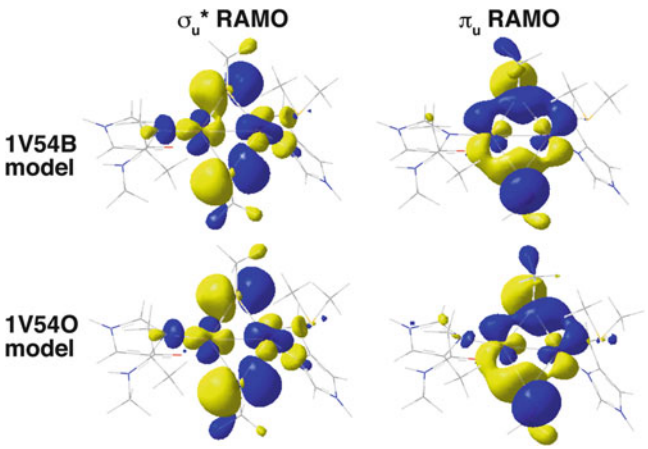

Fig. 30.4 σ_u* and π_u redox active molecular orbitals (RAMOs) of the 1V54B and 1V54O models of the Cu_A site in the gas phase. All isovalue surfaces are set at 0.03 $(e/Å^3)^{1/2}$. Molecular structures are shown in *thin lines*

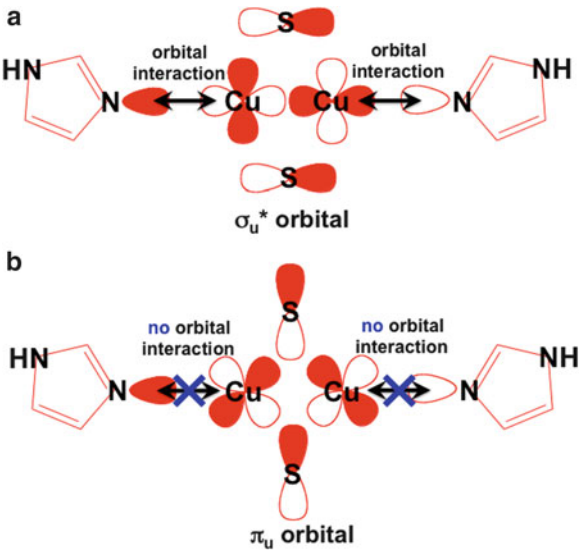

Fig. 30.5 Schematic pictures of the orbital interactions of the σ_u* (**a**) and π_u (**b**) orbitals of the Cu_2S_2 core with the His161 and His204 parts

are almost localized on only the Cu_2S_2 core, showing that the ligand coordination hardly affects the orbital energy of the π_u RAMOs. This difference in the orbital interactions between the Cu_2S_2 core and the coordinating ligands contributes to the higher orbital energy of the σ_u* RAMO, as compared with that of the π_u RAMO, resulting in the σ_u* ground state of the Cu_A site, as illustrated in Fig. 30.5. In addition, this stronger delocalized character of the σ_u* RAMO of the Cu_A site, as compared to the π_u RAMO, facilitates the overlapping of the molecular orbitals of the adjacent amino acids to accomplish the long electron transfer to heme *a* in C*c*O.

Although the geometrical parameters, in particular the Cu–Cu and S–S distances, are quite different between the 1V54B and 1V54O models (Fig. 30.3a), the shapes and symmetries of the σ_u* and π_u RAMOs are equivalent to each other. This orbital similarity results in the similarity in the electronic structures between two models. It indicates that the Cu_A site can transfer electrons despite the distortion of the diamond core, implying that the Cu_A site can be regarded as a "flexible electron mediator." This flexibility is useful for the incorporation of the Cu_A site to protein for electron transfer inside the protein. In the previous study [23], we exhibited that heme *a* in C*c*O can also keep the delocalized electronic structure in spite of the deformation of the porphyrin ring. These results indicate that metal cofactors, which are involved in the electron transfer in proteins, have such robustness of the delocalized state.

30.3.2 Spin Density Distribution of the Oxidized Cu_A Site

We next investigated the spin density distribution and Mulliken atomic spin densities of the 1V54B and 1V54O models in the σ_u* and π_u oxidized states, which show the

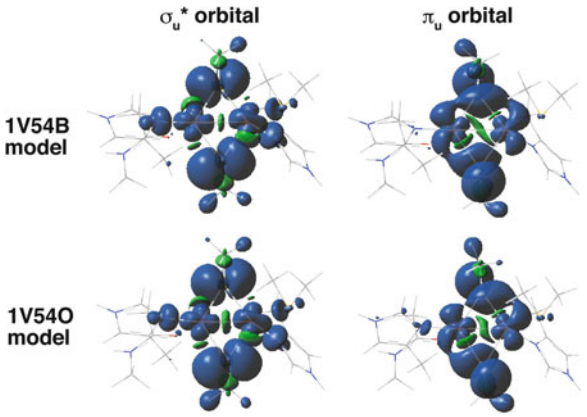

Fig. 30.6 Spin density distribution of the 1V54B and 1V54O models of the Cu_A site in the σ_u* and π_u oxidized states in the gas phase. All isovalue surfaces are set at 0.001 e/Å^3. Blue and green surfaces represent positive and negative spin densities, respectively. Molecular structures are shown in thin lines

character of the mixed-valence $Cu^{1.5+}$–$Cu^{1.5+}$ state. Since the oxidized state of the Cu_A site has an unpaired electron, the spin density distribution demonstrates that the positive spin density is fully delocalized over the Cu_2S_2 diamond core formed by the two copper ions and Cys196 and Cys200, and that the negative spin density polarized by the positive spin density is found on the chemical bonds such as the Cu–S and Cu–Cu bonds, as shown in Fig. 30.6.

The shapes of the spin density distribution are similar to those of RAMOs in both the σ_u* and π_u oxidized states, respectively, indicating that the SOMO is dominant to the mixed-valence $Cu^{1.5+}$–$Cu^{1.5+}$ character of the Cu_A site. While an unpaired electron is localized on one iron ion in the Fe^{3+}–Fe^{2+} mixed-valence active site of uteroferrin [29], due to the unsymmetrical coordination (class I mixed-valence state), it is fully delocalized over the Cu_2S_2 core of the models of the Cu_A site in both the σ_u* and π_u states. This means that the oxidized Cu_A site is a completely delocalized (class III) mixed-valence $Cu^{1.5+}$–$Cu^{1.5+}$ species even in the low-symmetry environment [42], because the direct bonding character of the copper ions is caused by the strong orbital interaction, leading to the strong delocalization over the Cu_2S_2 core in the Cu_A site.

As well as the RAMOs, the spin density distribution is delocalized on the directly coordinating N_δ and S_γ atoms of the His and Met residues in the σ_u* state, respectively, while it is almost localized over only the Cu_2S_2 diamond core in the π_u oxidized state. As listed in Table 30.1, the Mulliken atomic spin densities are found on the His161, His204, and Met207 parts in the σ_u* oxidized Cu_A models, whereas most of the Mulliken atomic spin densities are found on only the core part in the π_u oxidized ones. The RAMOs and spin density distribution supports the advantage of the σ_u* state in the electron transfer compared with the π_u state.

The spin density distribution and the Mulliken atomic spin densities of the 1V54B model are almost same as those of the 1V54O model, indicating the robust electronic structure of the Cu_A site and the synthetic model complexes; see Fig. 30.6 and Table 30.1.

Table 30.1 Mulliken atomic spin densities of the oxidized models (the 1V54B and 1V54 models) of the Cu_A site in the protein solution[a] at the M06 level of theory

	1V54B		1V54O	
Part	σ_u* oxidized	π_u oxidized	σ_u* oxidized	π_u oxidized
Core[b]	+0.890	+1.006	+0.891	+0.972
His161[b]	+0.047	−0.006	+0.039	+0.003
Glu198[b]	+0.003	+0.001	+0.002	+0.007
His204[b]	+0.033	−0.006	+0.040	+0.008
Met207[b]	+0.028	+0.005	+0.028	+0.009

[a]The protein solution was modeled by the PCM–UAKS method with the dielectric constant of 4.0
[b]The core, His161, Glu198, His204, and Met207 parts are shown in Fig. 30.3b. The Mulliken atomic spin densities in each part were summed up

Table 30.2 Mulliken atomic charge densities of the oxidized models (the 1V54B and 1V54O models) and the reduced models (the 1V55B and 1V54O models) of the Cu_A site in the protein solution[a] at the M06 level of theory

	1V54B		1V55B	1V54O		1V55O
Part	σ_u* oxidized	π_u oxidized	Reduced	σ_u* oxidized	π_u oxidized	Reduced
Core[b]	−0.312	−0.222	−0.672	+0.040	+0.105	−0.409
His161[b]	+0.541	+0.504	+0.416	+0.407	+0.374	+0.262
Glu198[b]	+0.088	+0.090	−0.056	+0.071	+0.071	−0.075
His204[b]	+0.620	+0.598	+0.352	+0.444	+0.442	+0.307
Met207[b]	+0.063	+0.030	−0.071	+0.038	+0.007	−0.085

[a]The protein solution was modeled by the PCM–UAKS method with the dielectric constant of 4.0
[b]The core, His161, Glu198, His204, and Met207 parts are shown in Fig. 30.3b. The Mulliken atomic charge densities in each part were summed up

30.3.3 Mulliken Atomic Charge Density of the Cu_A Site

Mulliken atomic charge densities are related to the distribution of all electrons of the Cu_A site. The computed Mulliken atomic charge densities are summarized in Table 30.2 and show that negative atomic charges move from the coordinating His198, His204, and Glu198 parts to the core part because the coordinating parts are electron-rich due to the unsaturated bonds of the imidazole ring of the His198 and His204 parts and the peptide group of the Glu198 part. Owing to the longest coordination distance, as shown in Fig. 30.3a, the Met207 part shows the smallest charge transfer to the core part in all the coordinating parts in the oxidized state and the back charge transfer in the reduced state. As compared to the Glu198 part, the stronger charge transfer of the His parts is responsible for the equatorially coordinating lone pair of the His161 and His204 parts to the core part (Fig. 30.5) and the weak axial coordination of the Glu198 part with the longer coordination distance of 2.4 Å, as shown in Fig. 30.3a.

Since the formal charges of the core part in the models of the Cu_A site are 1.0 and 0.0 in the oxidized and reduced states, respectively, the charge transfer of the models of the oxidized Cu_A site is much stronger than that of the reduced Cu $_A$ site. In the oxidized state, the charge transfer in the σ_u* state is stronger than that in the π_u state because the σ_u* orbital can interact with the lone pair of the His161 and His204 parts, while the π_u orbital fails to interact with them; see Fig. 30.5.

As compared with the 1V54O model, the 1V54B model provides the stronger ligand-to-core charge transfer, due to the change in the large amount of the negative charges of the His161 and His204 parts, as shown in Table 30.2. This result indicates that the stronger orbital interaction of the 1V54B model between the core and coordinating parts than the 1V54O model, resulting from the approach of the orbital energy of the RAMOs to that of the lone pair of the His part because the 0.14 Å longer Cu–Cu bond of the 1V54B model provides a weaker d–d antibonding interaction between the copper ions of the core part.

30.4 Concluding Remarks

By means of the M06 method with the PCM, we have explored the RAMOs, spin density distribution, and Mulliken atomic spin and charge densities of the models of the Cu_A site in the σ_u* and π_u states in order to elucidate the origin of the strong delocalized character of the oxidized σ_u* ground state in the Cu_A site. We found that the fully delocalized mixed-valence $Cu^{1.5+}$–$Cu^{1.5+}$ state of the Cu_A site is because the σ- and π-type direct orbital interactions are formed between the two copper ions and because the ligand coordination stabilizes the Cu–Cu direct interaction, as shown in Fig. 30.5a. The structural variation in the Cu_2S_2 core of the Cu_A site hardly influences the shape of the RAMO and spin density distribution, because broader 3d orbitals than 2p orbitals enable the direct orbital overlap between the two copper ions even in the Cu–Cu elongation by 0.14 Å [47]. It indicates that the charge densities can be strongly delocalized over the Cu_2S_2 core in the redox reaction, even when the Cu_2S_2 core is distorted. Since the charge delocalization is related to the electron transfer of the Cu_A site, the Cu_A site can transfer electrons despite the distortion of the Cu_2S_2 core. It implies that the Cu_A site can be regarded as a "flexible electron mediator." This flexibility is useful for the incorporation of the Cu_A site to protein for electron transfer inside the protein. The character of "flexible electron mediator" is found in not only heme *a* [23] but also the Cu_A site and is common to transition metal cofactors in biological electron transfer.

Acknowledgments This work was supported by grants from Research and Development of the Next-Generation Integrated Simulation of Living Matter, which is part of the Development and Use of the Next-Generation Supercomputer Project of MEXT. We are also grateful for a Grant-in-Aid for Scientific Research A (22685003) from JSPS and a Grant-in-Aid for Scientific Research on Innovative Areas "Materials Design through Computics" (23104506) from MEXT. The computations were performed at the Research Center for Computational Science, Okazaki, Japan, and the Cybermedia Center of Osaka University, Japan. The present study was performed under the Cooperative Research Program of the Institute for Protein Research, Osaka University.

References

1. Wilkström M (1977) Nature 266:271–273
2. Malmström BG (1990) Chem Rev 90:1247–1260
3. Ferguson-Miller S, Babcock GT (1996) Chem Rev 96:2889–2908
4. Malmström BG, Aasa R (1993) FEBS Lett 325:49–52
5. Solomon EI, Xie X, Dey A (2008) Chem Soc Rev 37:613–628
6. Savelieff MG, Lu Y (2010) J Biol Inorg Chem 15:416–483
7. Tsukihara T, Shimokawa K, Katayama Y, Shimada H, Muramoto K, Aoyama H, Mochizuki M, Shinzawa-Itoh K, Yamashita E, Yao M, Ishimura Y, Yoshikawa S (2003) Proc Natl Acad Sci USA 100:15304–15309
8. Blackburn NJ, Barr ME, Woodruff WH, van der Oost J, de Vries S (1994) Biochemistry 33:10401–10407
9. Farrar JA, Lappalainen P, Zumft WG, Saraste M, Thompson AJ (1995) Eur J Biochem 232:294–303
10. Gamelin DR, Randall DW, Hay MT, Houser RP, Mulder TC, Canters GW, de Vries S, Tolman WB, Lu Y, Solomon EI (1998) J Am Chem Soc 120:5246–5263
11. Froncisz W, Scholes CP, Hyde JS, Wei Y-H, King TE, Shaw RW, Beinert H (1979) J Biol Chem 254:7482–7484
12. Stevens TH, Martin CT, Wang H, Brudvig GW, Scholes CP, Chan SI (1982) J Biol Chem 257:12106–12113
13. Farrar JA, Neese F, Lappalainen P, Kroneck PMH, Saraste M, Zumft WG, Thomson AJ (1996) J Am Chem Soc 118:11501–11514
14. Kroneck PMH, Antholine WH, Riester J, Zumft WG (1988) FEBS Lett 242:70–74
15. Houser RP, Young VG, Tolman WB (1996) J Am Chem Soc 118:2101–2102
16. George SD, Metz M, Szilagyi RK, Wang H, Cramer SP, Lu Y, Tolman WB, Hedman B, Hodgson KO, Solomon EI (2001) J Am Chem Soc 123:5757–5767
17. Gennari M, Pécaut J, DeBeer S, Neese F, Collomb M-N, Duboc C (2011) Angew Chem Int Ed 50:5662–5666
18. Xie X, Gorelsky SI, Sarangi R, Garner DK, Hwang HJ, Hodgson KO, Hedman B, Lu Y, Solomon EI (2008) J Am Chem Soc 130:5194–5205
19. Olsson MHM, Ryde U (2001) J Am Chem Soc 123:7866–7876
20. Takano Y, Shigeta Y, Koizumi K, Nakamura H (2012) Int J Quantum Chem 112:208–218
21. Koizumi K, Shigeta Y, Okuyama O, Nakamura H, Takano Y (2012) Chem Phys Lett 531: 197–201
22. Takano Y, Nakamura H (2009) Int J Quantum Chem 109:3583–3591
23. Takano Y, Nakamura H (2010) J Comput Chem 31:954–962
24. Yamasaki H, Takano Y, Nakamura H (2008) J Phys Chem B 112:13923–13933
25. Takano Y, Yamaguchi K (2007) Int J Quantum Chem 107:3103–3119
26. Takano Y, Isobe H, Yamaguchi K (2008) Bull Chem Soc Jpn 81:91–102
27. Takano Y, Koizumi K, Yamaguchi K (2009) Inorg Chim Acta 362:4578–4584
28. Takano Y, Yonezawa Y, Fujita Y, Kurisu G, Nakamura H (2011) Chem Phys Lett 503:296–300
29. Koizumi K, Shoji M, Yamaguchi K, Nakamura H, Takano Y (2011) Int J Quantum Chem 111:702–710
30. Frisch MJ et al (2009) Gaussian 09. Gaussian, Inc., Wallingford
31. Becke AD (1993) J Chem Phys 98:1372–1377
32. Becke AD (1993) J Chem Phys 98:5648–5652
33. Becke AD (1988) Phys Rev A 38:3098–3100
34. Lee C, Yang W, Parr RG (1988) Phys Rev B 37:785–789
35. Perdew JP, Chevary JA, Vosko SH, Jackson KA, Pederson MR, Singh DJ, Fiolhais C (1992) Phys Rev B 46:6671–6687
36. Adamo C, Barone V (1999) J Chem Phys 110:6158–6169
37. Zhao Y, Truhlar DG (2008) Theor Chem Acc 120:215–241

38. Pople JA, Head-Gordon M, Raghavachari K (1987) J Chem Phys 87:5968–5975
39. Wachters AJH (1970) J Chem Phys 52:1033–1036
40. Hariharan PJ, Pople JA (1973) Theor Chem Acta 28:213–222
41. Hehre WJ, Ditchfild R, Pople JA (1972) J Chem Phys 56:2257–2261
42. Robin MB, Day P (1968) Adv Inorg Chem Radiochem 10:247–422
43. Cossi M, Scalmani G, Rega N, Barone V (2002) J Chem Phys 117:43–54
44. Takano Y, Houk KN (2005) J Chem Theory Comput 1:70–77
45. Gilson MK, Honig BH (1986) Biopolymers 25:2097–2119
46. Schutz CN, Warshel A (2001) Proteins 44:400–417
47. Atkins P, Friedman R (2005) Molecular quantum chemistry, 4th edn. Oxford, New York, pp 85–90